Journal of Magnetic Resonance **138,** 308–312 (1999)
Article ID jmre.1999.1756, available online at http://www.idealibrary.com on IDEAL®

COMMUNICATIONS

NMR Imaging of Thermally Polarized Helium-3 Gas

F. Kober, B. Koenigsberg, V. Belle, M. Viallon,* J. L. Leviel, A. Delon,† A. Ziegler, and M. Décorps

*INSERM U-438, Université Joseph Fourier, LRC CEA, LCHU, Pavillon B, BP217X, 38043 Grenoble, Cedex 9, France; *CNRS, UCB Lyon 1, Bat. 308, 69622 Villeurbanne, Cedex, France; and †LCMI, CNRS UPR 5021, 25 av. des Martyrs, BP166, 38042 Grenoble, Cedex 9, France*

E-mail: Michel.Decorps@ujf-grenoble.fr

Received February 4, 1998; revised February 24, 1999

It is shown that thermally polarized ^{3}He gas can be used to measure important physical parameters and to design, test, and tune imaging sequences. The bulk values of T_1, T_2, and the diffusion coefficient were measured in a glass cell containing a mixture of helium-3 (0.8 bar) and oxygen (0.2 bar). They were found to be $T_1 = 7$ s, $T_2 = 2.4$ s, and $D = 1.6$ cm^2 s^{-1}. The relaxation times T_2^* and T_1 and the apparent diffusion coefficient of thermally polarized helium-3 gas were measured in the rat lung, and these parameters were used to design a helium-3 optimized multi-spin–echo sequence which was shown to increase the signal-to-noise ratio sufficiently to obtain the first NMR-images of thermally polarized helium-3 in the rat lung.

Key Words: **NMR; MRI; helium; diffusion; lung imaging.**

Magnetic resonance imaging of hyperpolarized (*1*) gases promises to become an important method for pulmonary imaging (*1–12*). The unusual values of physical parameters of gases compared to those of water make the adaptation of imaging techniques necessary. Optimized imaging has to take into account a variety of major parameters. For ^{3}He, the T_1 values range from 10 to 50 s in helium/oxygen mixtures (*9, 12–14*) up to days in pure ^{3}He (*15*). The diffusion coefficient of ^{3}He at 300 K is on the order of 1–2 cm^2 s^{-1} (*16–18*), so up to 5 orders of magnitude greater than that for water protons. This limits the ultimate spatial resolution (*3, 19*) and induces signal loss in the presence of imaging gradients (*10, 16, 19*). Furthermore, susceptibility differences between gas and tissue give rise to microscopic field gradients, hence shortening both T_2^* and T_2 (*4, 20–23*). Restricted diffusion effects in the lung tissue can, however, strongly reduce the mean path of the gas atoms during imaging which would decrease diffusion–induced signal attenuation (*24*). To choose an imaging strategy and to optimize the signal-to-noise ratio, parameter measurement is necessary.

Lung gas phase imaging at thermal polarization level was recently demonstrated in the rat using an inert fluorinated gas (*25*). In this work, we show that the thermal polarization of ^{3}He at room temperature is sufficient for measuring the major parameters of ^{3}He within reasonable experiment times in a glass cell at atmospheric pressure as well as in the rat lung. We show that careful design of the imaging sequence with respect to the parameter measurements allows imaging of the rat lung with ^{3}He in thermal equilibrium. Thus, measurement of important physical parameters such as relaxation and diffusion data, as well as design, optimization, and tuning of MRI techniques, can be carried out with thermally polarized gas rather than with hyperpolarized gas, allowing one to prepare the way for more sensitive experiments with laser polarized gas.

All measurements were performed in a BRUKER 2.35 T magnet (40 cm bore) using a SMIS imaging system. We used an Alderman–Grant rf-coil resonant at 76 MHz for ^{3}He and at 100 MHz for ^{1}H. For the phantom studies, we used a Pyrex glass cell of 48 cm^3 filled with a mixture of ^{3}He ($p_{He} = 0.8$ bar) and O_2 ($p_{O_2} = 0.2$ bar). All experiments were carried out at room temperature (21°C). The T_1 value of the mixture was determined using a saturation-recovery technique. The result was $T_1 = 10 \pm 1$ s. T_2 was obtained using a CPMG sequence. We have acquired 64 echoes. The inter-echo time was chosen to be 640 μs in order to avoid the influence of diffusion in the possibly inhomogeneous static field. We obtained a T_2 value of 2.4 ± 0.2 s. The diffusion coefficient D was measured using a spin–echo method (Fig. 1). We acquired 16 echoes with increasing gradient strength, $G_i = i\Delta G$ with $i = 1, \ldots, 16$. The signal attenuation $A(G_i)$ is given by the Stejskal–Tanner equation,

$$A(G_i) = \exp\left(-\frac{2}{3}\gamma^2 D G_i^2 \delta^3\right), \qquad [1]$$

where δ is the gradient duration and γ is the ^{3}He gyromagnetic ratio. D was obtained from a nonlinear least-squares adjustment of Eq. [1] over the experimental echo amplitudes. Figure 2 shows the measurement data as well as the fitted theoretical decay. The measured attenuation curve shows good agreement

1090-7807/99 $30.00

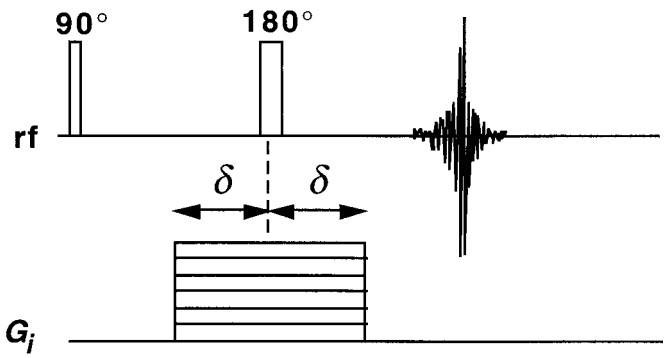

FIG. 1. Sequence used for the diffusion coefficient measurement in the cell. The gradient duration δ was 5 ms, the diffusion gradient increment $\gamma\Delta G/2\pi = 47.5$ Hz cm^{-1} and the repetition time 60 s. The 180° pulse was applied in the presence of the diffusion gradient. The pulse length of the 180° pulse was 100 μs so that its bandwidth was large enough to refocus all spins in the cell homogeneously at the maximum gradient value.

with Eq. [1]. The resulting diffusion coefficient was $D = 1.60 \pm 0.05$ cm^2 s^{-1}. This value was also found in good agreement with the value $D = 1.51$ cm^2 s^{-1}, calculated at 1 atm from the diffusion coefficient measured at 3.6 atm in an ^{3}He/O_2 mixture at thermal equilibrium with a 27% O_2 fraction (*16*), assuming that gas coefficients scale inversely with gas pressure (*26*). As expected, the diffusion coefficient of the ^{3}He/O_2 mixture was found to be smaller than that of pure ^{3}He at 1 atm and room temperature which was reported to be $D = 1.96$ cm^2 s^{-1} (*17*) from techniques other than NMR, whereas a recent NMR measurement (*16*) in a hyperpolarized sample at 1 atm yields a value of $D = 1.87$ cm^2 s^{-1}.

A preliminary animal experiment was performed using the same imaging system and helium rf-coil as described above. The rat was anesthetized (halothane 1%), tracheotomized, and mechanically ventilated. Normal saline containing pancuronium bromide (0.04 mg/ml) was infused intreperitoneally at a rate of 1–2 ml/h throughout the study. After positioning, a proton gradient-echo image was acquired. Before ^{3}He breathing, the animal was ventilated with pure oxygen for 10 min. Anesthesia was maintained with halothane (1%). Then three breaths of ^{3}He were used in order to wash out the residual oxygen in the lungs. The rat was then held in apnea. During this first apnea phase, we measured the T_1 value using a saturation-recovery technique (duration 3 min) as well as T_2^*. Then, the normal ventilation (air/halothane) was continued for 20 min followed by a period of 10 min of ventilation with pure oxygen. After washing out the residual oxygen in the lungs, the rat was held in apnea for 8 min to acquire a transverse image of the rat lung. At the end of the experiment, the rat was euthanized with an overdose of halothane.

The relaxation time T_1 was measured to be 35 s. From linewidth measurements, a value of $T_2^* = 2$ ms was found in the rat lung. This value is shorter than the results recently reported in the live guinea pig lung from spatially resolved measurements ($T_2^* \approx 11$–16 ms) at 2 T (*22*). Thus, the decreased value is most probably due to insufficient magnet shimming. However, bulk magnetic susceptibility effects could contribute to line-broadening in this nonlocalized measurement. The short T_2^* value requires adapted acquisition times per excitation. On the other hand, susceptibility gradients in the rat lung coupled to rapid diffusion of ^{3}He could reduce significantly the apparent T_2. It was previously shown, however, that the observed T_2 of ^{129}Xe in the rat lung was long enough for multi-spin–echo sequences (*23*). Similarly, for helium gas in the human lung at low field, T_2 was found as large as 6 s when measured with a CPMG sequence at 30 ms inter-echo time, suggesting motional narrowing (*9*). Finally, it was shown that projection imaging minimizes signal loss due to diffusive motion in the presence of imaging gradients (*5*). Thus, we have chosen a multi-spin–echo projection–reconstruction technique (Fig. 3) which allows a very short echo time to be used. In our current implementation, no slice selection was performed. This could be introduced by using selective refocusing pulses in combination with slice gradients, but would require rapid gradient commutation. No signal averaging was performed in any of the experiments. The data set was first used to estimate the apparent diffusion coefficient D_{app} in the rat lung as the sequence represents a repeated Stejskal–Tanner experiment. Assuming a negligible T_2 decay during the echo train, the signal attenuation at the center of the nth echo is given by

$$A_n = \exp\left(-\frac{1}{12}\gamma^2 D_{app} G_r^2 T_E^3 n\right), \qquad [2]$$

where T_E is the inter-echo time. G_r is the projection-gradient strength which was 44 μT cm^{-1} in our experiment. From the exponential decay of the echo amplitude with the echo number, the apparent diffusion coefficient D_{app} can be measured. D_{app} was obtained by fitting Eq. [2] to the measured echo ampli-

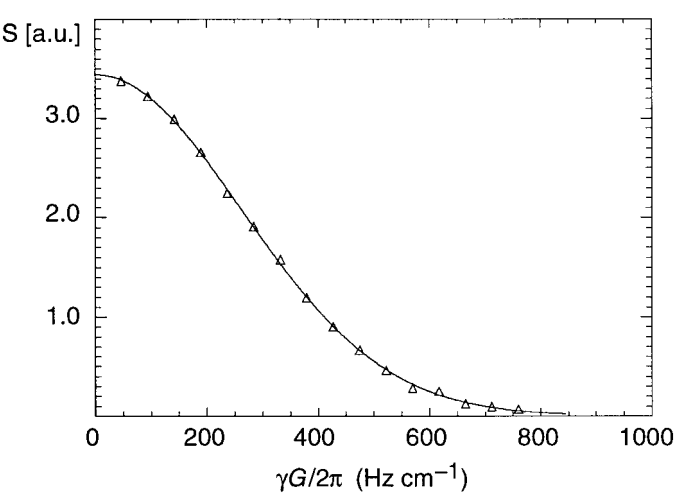

FIG. 2. Least-squares fit (line plot) of the function given by Eq. [1] to the spin–echo amplitudes (triangles) for ^{3}He diffusion coefficient D measurement.

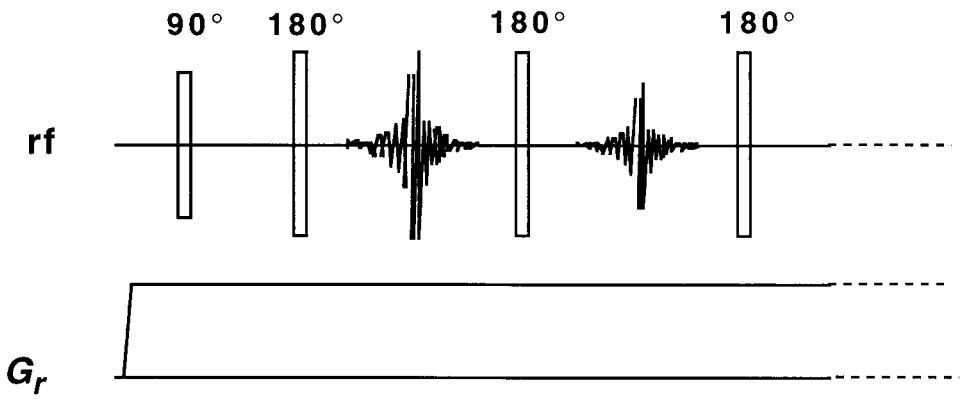

FIG. 3. Multi-echo projection–reconstruction sequence used for lung imaging. The orientation of the projection-gradient G_r is rotated at each excitation. 16 projections with 64 echoes each were acquired. From each echo, 16 data points were collected. The acquisition time was chosen to be 1.6 ms for each echo and the inter-echo time was 2.5 ms. The field-of-view was 7 cm.

tudes. The fit result for D_{app} is shown in Fig. 4. The experimental points do not decay perfectly exponentially. This multiexponential behavior could reflect the presence of compartments with different sizes (for example, alveoli and trachea). Refocusing-pulse imperfections leading to a steady state could also introduce some nonexponential decay. We can, however, give the result as an estimation of D_{app} during the inter-echo time T_E: $D_{app} \approx 0.4\ cm^2\ s^{-1}$. The difference between the diffusion coefficient of helium in the phantom and the alveolar tissue is probably due to restricted diffusion (*24*).

For image reconstruction, we performed a weighted summation of the echoes using

$$S(t) = \sum_{n=1}^{N} W_n B_n(t), \qquad [3]$$

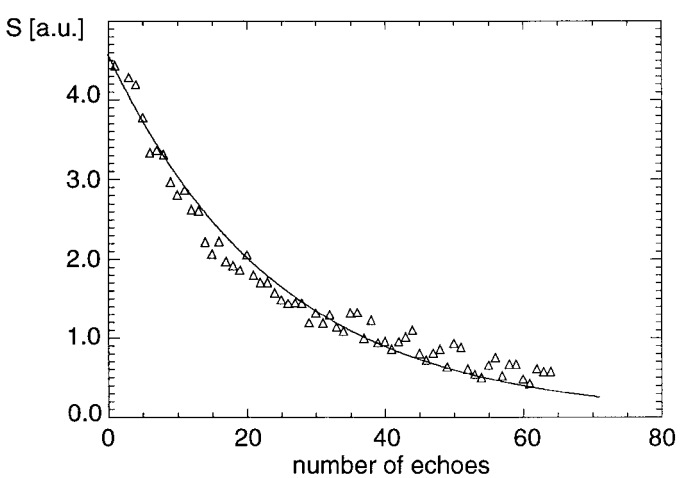

FIG. 4. Measurement of the apparent diffusion coefficient D_{app} in the rat lung. Triangles, experimental echo amplitudes; line-plot, fit result for the function (*2*).

where $B_n(t)$ is the nth echo of each echo train and $S(t)$ the weighted signal sum. N is the number of echoes to be summed. W_n represents a matched weighting function. Using the Cauchy–Schwartz inequality, it is easy to show that optimum weighting regarding signal-to-noise ratio is achieved by setting $W_n = S_n$, where S_n is the amplitude of the nth echo which is given by Eq. [2] for $D_{app} = 0.4\ cm^2\ s^{-1}$. This result is widely used in NMR spectroscopy for example when a FID is multiplied by an exponentially decaying function with a time constant T_2^*. Images were obtained by interpolation of the k-space data on a rectilinear grid, zerofilling, 2D-Fourier transformation, and modulus calculation. Taking into account the overall size of the rat lung (about FOV/3), it should be noted that the data is significantly oversampled both in the radial direction (by a factor of 3) and in the angular direction (by a factor of $6/\pi$). In Fig. 5, the reconstructed images for $N = 1$, 4, 16, and 64 are displayed. The images show that a significant gain in signal-to-noise ratio can be obtained by using the proposed multi-spin–echo technique which takes advantage of the long T_2 value. The 64-echo image (Fig. 5d) can be compared to the proton image (Fig. 5e). The two lungs as well as the position of the heart can be identified in the helium image.

We have shown that NMR measurement of physical parameters is possible in thermally polarized ^{3}He. Important parameters for the design of pulse sequences have been measured for ^{3}He in the rat lung. Taking into account the measured parameters, we were able to obtain the first thermally polarized ^{3}He images of the rat lung. The use of an optimized multi-echo projection–reconstruction sequence allowed us to obtain a sufficient signal-to-noise ratio with a total imaging time of 8 min and an in-plane resolution of $4.4 \times 4.4\ mm^2$. The imaging time could be significantly reduced by using ^{3}He/O_2 mixtures which would offer the advantage of a reduced T_1, allowing shorter repetition times to be used. The same technique could be used

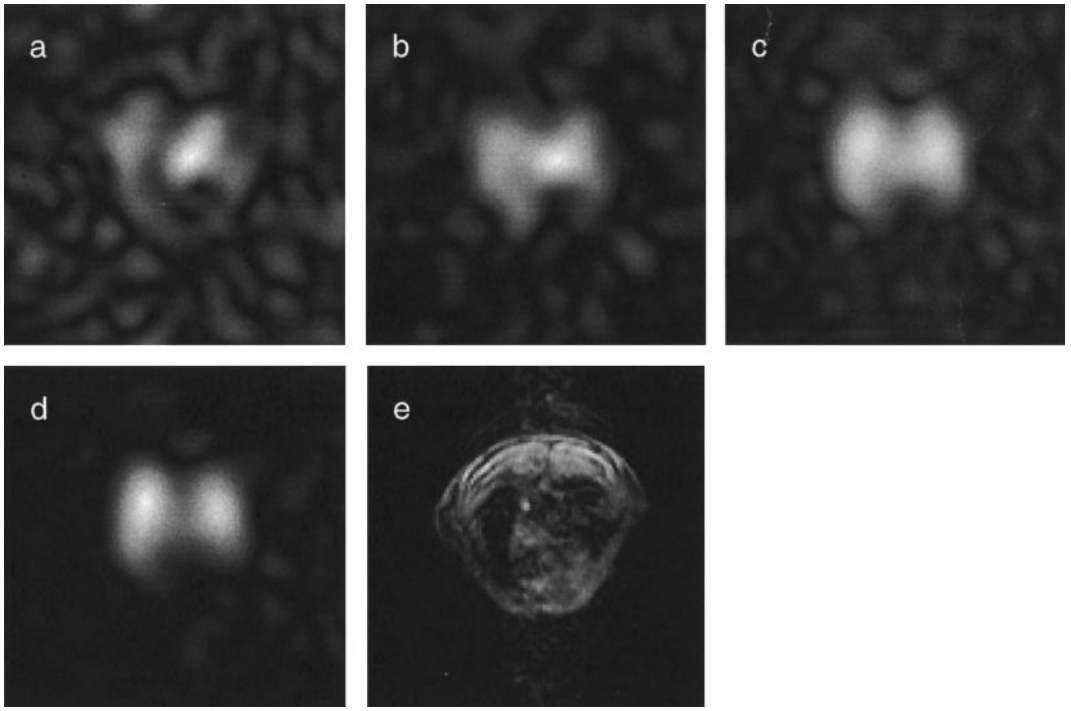

FIG. 5. Transverse ^{3}He images of the rat lung reconstructed from weighted signal sums: (a) $N = 1$, (b) $N = 4$, (c) $N = 16$, (d) $N = 64$. (e) FLASH proton image (128 × 64 pixels, field-of-view 7 × 7 cm^2, slice thickness 5 mm).

under normal ventilation conditions. It should be noted that a similar technique was recently exploited with hyperpolarized ^{3}He to obtain human lung images (*27*). Since the first demonstration (*1*), lung imaging with laser polarized gas has stimulated great interest for both clinical applications (*2, 3, 5, 7, 9, 14*) and animal model studies (*4–6, 10, 11, 28–32*). The use of thermally polarized gas could be of great help for optimizing the MRI strategy.

ACKNOWLEDGMENTS

The authors thank Timur Ünlü for helpful discussions. This work was supported by a BQR grant of the University Joseph Fourier, Grenoble.

REFERENCES

1. M. S. Albert, G. D. Cates, B. Driehuys, W. Happer, B. T. Saam, C. S. Springer Jr, and A. Wishnia, Biological magnetic resonance imaging using laser-polarized 129Xe, *Nature* **370,** 199–201 (1994).
2. M. Ebert, T. Grossman, W. Heil, E. W. Otten, R. Surkau, M. Leduc, P. Bachert, M. Knopp, L. Schad, and M. Thelen, Nuclear magnetic resonance imaging with hyperpolarized helium-3, *Lancet* **347,** 1297–1299 (1996).
3. J. R. MacFall, H. C. Charles, R. D. Black, H. L. Middleton, J. C. Swartz, B. T. Saam, B. Driehuys, C. Erickson, W. Happer, G. D. Cates, G. A. Johnson, and C. E. Ravin, Human lung air spaces: potential for MR imaging with hyperpolarized He-3, *Radiology* **200,** 553–558 (1996).
4. X. J. Chen, M. S. Chawla, G. P. Cofer, L. W. Hedlund, H. E. Möller, and G. A. Johnson, Hyperpolarized ^{3}He NMR lineshape measurements in the live guinea pig lung, *Magn. Reson. Med.* **40,** 61–65 (1998).
5. X. J. Chen, M. S. Chawla, L. W. Hedlund, H. E. Möller, J. R. MacFall, and G. A. Johnson, MR microscopy of lung airways with hyperpolarized ^{3}He, *Magn. Reson. Med.* **39,** 79–84 (1998).
6. H. L. Middleton, R. D. Black, B. T. Saam, G. D. Cates, G. P. Cofer, R. Guenther, W. Happer, L. W. Hedlund, G. A. Johnson, K. Juvan, and J. C. Swartz, MR imaging with hyperpolarized ^{3}He gas, *Magn. Reson. Med.* **33,** 271–275 (1995).
7. H.-U. Kauczor, D. Hofmann, K.-F. Kreitner, H. Nilgens, R. Surkau, W. Heil, A. Potthast, M. Knopp, E. W. Otten, and M. Thelen, Normal and abnormal pulmonary ventilation: visualization at hyperpolarized He-3 MR imaging, *Radiology* **201,** 564–568 (1996).
8. J. R. MacFall, H. C. Charles, R. D. Black, H. L. Middleton, J. C. Swartz, B. T. Saam, W. Happer, G. D. Cates, G. A. Johnson, and C. E. Ravin, MR imaging of lung air spaces with hyperpolarized ^{3}He, *in* "Proceedings of the 4th Annual Meeting of the Society of Magnetic Resonance, New York, April 27–May 3, 1996."
9. L. Darrasse, G. Guillot, P.-J. Nacher, and G. Tastevin, Low-field ^{3}He nuclear magnetic resonance in human lungs, *CR Acad. Sci. IIB* **324,** 691–710 (1997).
10. G. A. Johnson, G. Cates, X. J. Chen, G. P. Cofer, B. Driehuys, W. Happer, L. W. Hedlund, B. Saam, M. D. Shattuck, and J. Swartz, Dynamics of magnetization in hyperpolarized gas MRI of the lungs, *Magn. Reson. Med.* **38,** 66–71 (1997).
11. Y. Crémillieux, Y. Berthezène, H. Humblot, M. Viallon, E. Canet, M. Bourgeois, T. Albert, W. Heil, and A. Briguet, A combined ^{1}H perfusion/^{3}He ventilation NMR study in rat lungs, *Magn. Reson. Med.,* in press.
12. H. E. Möller, X. J. Chen, M. S. Chawla, B. Driehuys, L. W. Hedlund, and G. A. Johnson, Signal dynamics in magnetic resonance imag-

ing of the lung with hyperpolarized noble gases, *J. Magn. Reson.* **135,** 133–143 (1998).

13. B. T. Saam, W. Happer, and H. L. Middleton, Nuclear relaxation of ^{3}He in the presence of O_2, *Phys. Rev. A* **52,** 862–865 (1995).
14. P. Bachert, L. Schad, M. Bock, M. Knopp, M. Ebert, T. Grossman, W. Heil, D. Hofmann, R. Surkau, and E. W. Otten, Nuclear magnetic resonance imaging of airways in humans with use of hyperpolarized ^{3}He, *Magn. Reson. Med.* **36,** 192–196 (1996).
15. W. Heil, H. Humblot, E. W. Otten, M. Schaefer, R. Sarkau, and M. Leduc, Very long nuclear relaxation times of spin polarized helium 3 in metal coated cells, *Phys. Lett. A* **201,** 337–343 (1995).
16. M. Bock, Simultaneous T_2^* and diffusion measurements with ^{3}He, *Magn. Reson. Med.* **38,** 890–895 (1997).
17. D. M. Schmidt, J. S. George, S. I. Pentilla, A. Caprihan, and E. Fukushima, Diffusion imaging with hyperpolarized ^{3}He gas, *J. Magn. Reson.* **129,** 184–187 (1997).
18. R. Barbé, M. Leduc, and F. Laloë, Résonance magnétique en champ de radiofréquence inhomogène. II. Vérifications expérimentales; mesure du coefficient de self-diffusion de ^{3}He, *J. Phys.* **35,** 935–951 (1974).
19. J.-H. Gao, L. Lemen, J. Xiong, B. Patyal, and P. T. Fox, Magnetization and diffusion effects in NMR imaging of hyperpolarized substances, *Magn. Reson. Med.* **37,** 153–158 (1997).
20. C. J. Bergin, G. H. Glover, and J. M. Pauly, Lung parenchyma: Magnetic susceptibility in MR imaging, *Radiology* **180,** 845–848 (1991).
21. R. A. Christman, D. C. Ailion, T. A. Case, C. H. Durney, A. G. Cutillo, S. Shioya, K. C. Goodrich, and A. H. Morris, Comparison of calculated and experimental NMR spectral broadening for lung tissue, *Magn. Reson. Med.* **35,** 6–13 (1996).
22. X. J. Chen, M. S. Chawla, G. P. Cofer, B. Driehuys, L. W. Hedlund, J. R. MacFall, H. E. Möller, and G. A. Johnson, Spatially localized T_2^* measurements of hyperpolarized ^{3}He in the lung, *in* "Proceedings of the 6th Scientific Meeting of the International Society of Magnetic Resonance in Medicine, Sydney (Australia), April 18–24, 1998."
23. L. Zhao, R. V. Mulkern, A. Venkatesh, H. Gudbjartsson, F. A. Jolesz, and M. S. Albert, Hyperpolarized ^{129}Xe T_2 and diffusion measurements for fast spin–echo MRI, *in* "Proceedings of the 6th Scientific Meeting of the International Society of Magnetic Resonance in Medicine, Sydney (Australia), April 18–24, 1998."
24. T. Maier, J. Knight-Scott, V. Mai, J. Mugler III, and J. Brookeman, Restricted diffusion of hyperpolarized ^{3}He in the human lung, *in* "Proceedings of the 6th Scientific Meeting of the International Society of Magnetic Resonance in Medicine, Sydney (Australia), April 18–24, 1998."
25. D. O. Kuethe, A. Caprihan, E. Fukushima, and R. A. Waggoner, Imaging lungs using inert fluorinated gases, *Magn. Reson. Med.* **39,** 85–88 (1998).
26. R. W. Mair, D. G. Cory, S. Peled, C.-H. Tseng, S. Patz, and R. L. Walsworth, Pulsed-field-gradient measurements of time-dependant gas diffusion, *J. Magn. Reson.* **135,** 478–486 (1998).
27. L. Darrasse, G. Guillot, P. Nacher, and G. Tastevin, Low field single shot ^{3}He MRI in human lungs, *in* "Proceedings of the 6th Scientific Meeting of the International Society of Magnetic Resonance in Medicine, Sydney (Australia), April 18–24, 1998."
28. M. E. Wagshul, T. M. Button, H. F. Li, Z. Liang, K. Zhong, and A. Wishnia, In vivo MR imaging and spectroscopy using hyperpolarized ^{129}Xe, *Magn. Reson. Med.* **36,** 183–191 (1996).
29. R. D. Black, H. L. Middleton, G. D. Cates, G. P. Cofer, B. Driehuys, W. Happer, L. W. Hedlund, G. A. Johnson, M. D. Shattuck, and J. C. Swartz, In vivo He-3 MR images of guinea pig lungs, *Radiology* **199,** 867–870 (1996).
30. M. D. Shattuck, S. L. Gewalt, G. H. Glover, L. W. Hedlund, and G. A. Johnson, MR microimaging of the lung using volume projection encoding, *Magn. Reson. Med.* **38,** 938–942 (1997).
31. K. Sakai, A. Bilek, E. Oteiza, R. L. Walsworth, D. Balamore, F. A. Jolesz, and M. S. Albert, Temporal dynamics of hyperpolarized ^{129}Xe resonances in living rats, *J. Magn. Reson. B* **111,** 300–304 (1996).
32. S. L. Gewalt, G. H. Glover, L. W. Hedlund, G. P. Cofer, J. R. MacFall, and G. A. Johnson, MR microscopy of the rat lung using projection reconstruction, *Magn. Reson. Med.* **29,** 99–106 (1993).